Nonlinear Stabilization of Tokamak Microturbulence by Fast Ions

J. Citrin,[1,4,*] F. Jenko,[2] P. Mantica,[3] D. Told,[2] C. Bourdelle,[4] J. Garcia,[4] J. W. Haverkort,[5,1] G. M. D. Hogeweij,[1] T. Johnson,[6] and M. J. Pueschel[7]

[1]*FOM Institute DIFFER—Dutch Institute for Fundamental Energy Research, Association EURATOM-FOM, Trilateral Euregio Cluster, PO Box 1207, 3430 BE Nieuwegein, The Netherlands*

[2]*Max Planck Institute for Plasma Physics, EURATOM Association, 85748 Garching, Germany*

[3]*Istituto di Fisica del Plasma "P. Caldirola," Associazione Euratom-ENEA-CNR, Milano, Italy*

[4]*CEA, IRFM, F-13108 Saint Paul Lez Durance, France*

[5]*Centrum Wiskunde and Informatica (CWI), PO Box 94079, 1090 GB Amsterdam, Netherlands*

[6]*Euratom-VR Association, EES, KTH, Stockholm, Sweden*

[7]*University of Wisconsin-Madison, Madison, Wisconsin 53706, USA*

(Received 21 June 2013; published 7 October 2013)

Nonlinear electromagnetic stabilization by suprathermal pressure gradients found in specific regimes is shown to be a key factor in reducing tokamak microturbulence, augmenting significantly the thermal pressure electromagnetic stabilization. Based on nonlinear gyrokinetic simulations investigating a set of ion heat transport experiments on the JET tokamak, described by Mantica *et al.* [Phys. Rev. Lett. **107**, 135004 (2011)], this result explains the experimentally observed ion heat flux and stiffness reduction. These findings are expected to improve the extrapolation of advanced tokamak scenarios to reactor relevant regimes.

DOI: 10.1103/PhysRevLett.111.155001 PACS numbers: 52.30.Gz, 52.35.Ra, 52.55.Fa, 52.65.Tt

Introduction.—It has been well established that a significant limiting factor of core energy confinement in tokamaks is turbulent transport driven by microinstabilities [1]. The ion-temperature-gradient (ITG) instability [2] has long been identified as an important driver of microturbulence, and is primarily responsible for ion heat losses. ITG modes are driven linearly unstable by logarithmic ion temperature gradients above a critical threshold, i.e., by $R/L_{Ti} > R/L_{Ti,\mathrm{crit}}$, where the tokamak major radius R is a normalizing factor. The modes saturate in conjunction with nonlinearly excited zonal flows, forming a self-organized turbulent system which sets the transport fluxes [3]. In the following, we term "stiffness" the degree of sensitivity of the ion heat flux to the driving R/L_{Ti}. At lower stiffness, higher R/L_{Ti} is attained for the same input heat flux and critical threshold.

Improving core confinement by mechanisms which increase the instability critical thresholds and/or decrease the temperature profile stiffness would increase fusion power in reactors, ultimately reducing the electricity cost. This Letter discusses such a mechanism—nonlinear electromagnetic stabilization of ITG turbulence by thermal and suprathermal pressure gradients—as modeled in simulations and in agreement with experimental observations. This specific effect is most relevant for "hybrid scenarios," an advanced operating regime developed on present-day tokamaks which may extrapolate favorably to future devices such as ITER [4,5].

The motivation for this study stems from recent experiments where a significant reduction of ion stiffness was reported in conditions of concomitant low magnetic shear $\hat{s}$ and high rotational flow shear. [6,7]. However, until now, nonlinear gyrokinetic simulations have not reproduced the stiffness reduction. $\hat{s} \equiv (r/q)(dq/dr)$, where q is the "safety factor" profile which increases with the ratio between the toroidal and poloidal magnetic fields.

We report on gyrokinetic simulations of discharges reported in Ref. [7], using the GENE code [8]. Nonlinear stabilization of ITG turbulence by thermal and suprathermal pressure gradients significantly reduces the simulated ion heat flux to levels consistent with the measured values, explaining the observed stiffness reduction. This stabilization mechanism is shown to be more effective at low $\hat{s}$, in agreement with observations. The rotational flow shear is seen *not* to be an important stabilizing factor in this regime. By "stabilization" we mean a reduction, rather than a full suppression, of mode growth rates (in linear simulations) or ion heat flux (in nonlinear simulations), when including the additional physics.

Previously considered *linear* mechanisms of fast ion stabilization of ITG modes include fast ion dilution of the main ion species [9,10], Shafranov shift stabilization [11], and electromagnetic (i.e., including both electric and magnetic field fluctuations in the model) stabilization by suprathermal pressure gradients [12]. For our discharge parameters, the nonlinear stabilization when including the first two effects scales with the degree of linear stabilization. However, the degree of nonlinear electromagnetic stabilization is significantly greater than the linear case. This *nonlinear* enhancement is the key factor that explains the experimental results.

Experimental discharges.—A subset of discharges described in Ref. [7] is analyzed at $\rho = 0.33$, where ρ is

 © 2013 American Physical Society

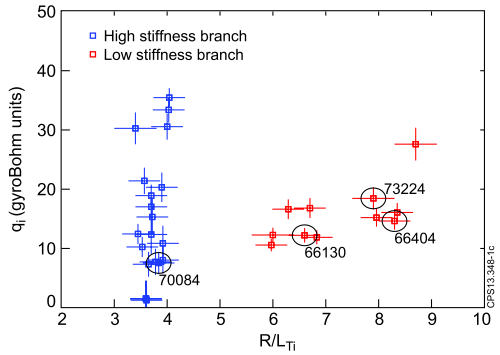

FIG. 1 (color online). Ion heat flux versus R/L_{Ti}, from JET data presented in Ref. [7] showing a separation between high and low stiffness regimes at $\rho = 0.33$. The specific discharges studied in this Letter are circled.

the normalized square root of the toroidal flux. The data split into two branches corresponding to high and low stiffness, separated by the heating scheme. While the discharges in both branches utilize ion cyclotron resonance heating (ICRH), the discharges in the "low stiffness" branch also utilize significant neutral beam injection (NBI). We concentrate on the low stiffness branch, and the specific discharges studied are circled in Fig. 1. The reduced stiffness is evident both from modulation experiments and from measured R/L_{Ti}, which are significantly greater than the modeled linear instability thresholds. We note, however, that the ion heat transport in discharge 66404 has been analyzed in Ref. [13], and the possibility of increased critical threshold also contributing to the observation is not ruled out. The correlation between reduced stiffness and low $\hat{s}$ is reported in Ref. [7].

The fast ion profiles were calculated by the NEMO/SPOT code [14] for NBI-driven fast ions and by the SELFO code [15] for the ICRH-driven fast ions (^{3}He). SELFO includes finite ion cyclotron orbit width effects, important for an accurate calculation of the ICRH fast ion pressure profile width. Interpretative simulations of the discharges with the CRONOS [16] code yielded safety factor q and $\hat{s}$ values within $\approx 15\%$ of the motional Stark effect or polarimetry constrained EFIT equilibrium code calculations. The discharge dimensionless parameters fed into the nonlinear gyrokinetic calculations are summarized in Table I. Details of the heating schemes used are in Ref. [6]. The ion heat flux and stiffness sensitivity to the various parameters were extensively studied, and the key parameters which impact the stiffness in this parameter regime are β_e and the fast ion profiles.

Simulation setup.—The gyrokinetic turbulence code GENE was used in the radially local limit, justified since here $1/\rho^* \approx 500$ [17,18]. ρ^* is the ion Larmor radius normalized to the tokamak minor radius. Typical GENE grid parameters were as follows: perpendicular box sizes $[L_x, L_y] = [170, 125]$ in units of $\rho_s \equiv c_s/\Omega_{ci}$, perpendicular grid discretizations $[n_x, n_y] = [192, 48]$, $n_z = 24$ points in the parallel direction, 32 points in the parallel velocity direction, and 8 magnetic moments. $c_s \equiv (T_e/m_i)^{1/2}$ and $\Omega_{ci} \equiv (eB/m_i)$. x is the GENE radial coordinate, z the coordinate along the field line, and y the binormal coordinate. All simulations included kinetic electrons. Both an analytical circular geometry model [19] as well as an experimental geometry were used. Extensive convergence tests were carried out throughout the parameter space spanned.

The ion heat fluxes correspond to time-averaged values over the saturated state of the simulations, and are in gyroBohm normalized units. The normalizing factor is $q_{iGB} = T_i^{2.5} n_i m_i^{0.5}/e^2 B^2 R^2$, where n_i is the ion density and m_i the ion mass. However, for consistency with Refs. [6,7], n_e was used as a proxy for n_i in the normalization in this work. For purely toroidal rotational flow shear, as assumed here, $\gamma_E \equiv (r/q)(d\Omega/dr)/(c_s/R)$ is the normalized perpendicular flow shear rate. In the electromagnetic simulations, only the $\delta B_\perp$ fluctuations were computed, justified by the relatively low β_e values. Including $\delta B_\parallel$ in the system had a negligible impact on the heat flux.

Impact of flow shear.—The high and low stiffness branches are correlated with low ($\gamma_E \approx 0.1$) and high (0.3)

TABLE I. Discharge dimensionless parameters at $\rho = 0.33$, analyzed in a quasistationary state at flattop. For brevity, only error bars for parameters which have significant impact on the system in the parameter range studied are displayed. The errors are statistical and do not take into account any systematic errors. $T_{(e,i)}$ are the electron and ion temperatures, $R/L_{(T,n)}$ the normalized logarithmic temperature and density gradients, $\beta_e \equiv p_e/(B^2/2\mu_0)$, the ratio between the thermal electron and magnetic pressure, and ν^* is the electron-ion collision frequency normalized to the trapped electron bounce frequency. The R/L_{Ti} values differ from Fig. 1 due to a different profile analysis technique used in this work compared with Ref. [7]. However, the respective values agree within their confidence intervals.

Shot	$\hat{s}$	q	T_e/T_i	R/L_{Ti}	R/L_{Te}	R/L_{ne}	β_e [%]	ν^*
70084	0.7	1.7	1.08 ± 0.04	3.5 ± 0.5	3.8	1.4	0.19 ± 0.01	0.07
66130	0.7	1.8	1.25 ± 0.13	6 ± 0.4	6.5	2.4	0.46 ± 0.09	0.04
66404	0.4	1.8	1.14 ± 0.06	8.6 ± 0.9	5.5	3.8	0.35 ± 0.07	0.02
73224	0.5	1.7	1.0 ± 0.02	9.3 ± 1	6.8	1.3	0.33 ± 0.004	0.038

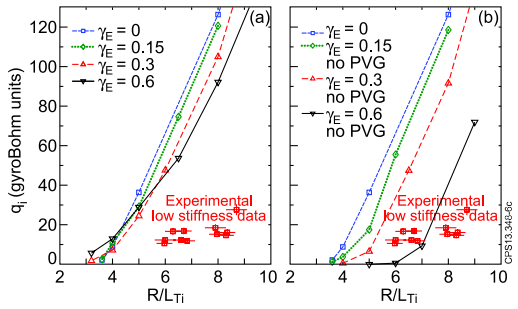

FIG. 2 (color online). Ion heat flux in nonlinear GENE R/L_{Ti} and γ_E scans based on discharge 70084 parameters at $\rho = 0.33$ ($q/\epsilon = 11.8$ for circular geometry). $\hat{s}/q = 0.2/1.3$ throughout. Results are shown both including (a) and neglecting (b) PVG destabilization. All runs were electrostatic, collisionless, used circular geometry, and assumed $T_e/T_i = 1$. The results are compared with the low stiffness data from Ref. [7].

flow shear, respectively. This correlation, together with concomitant low $\hat{s}$, was previously hypothesized to lead to the stiffness reduction. However, as shown in Fig. 2, the modeled impact of the flow shear on the ion heat flux was not sufficient to reduce the flux level and stiffness to the experimental values. $\hat{s} = 0.2$ in the scans, chosen to test the flow shear stabilization impact in the lower range of reasonable variations from the nominal value. Scans at the nominal $\hat{s}$ and q values also did not reproduce the experimental observations.

The impact of parallel velocity gradient (PVG) destabilization is significant. The PVG drive increases with increasing geometrical factor q/ϵ [20,21], where $\epsilon \equiv r/R$ is the local inverse tokamak aspect ratio. For our parameters, PVG destabilization strongly counteracts the $E \times B$ stabilization, as seen by comparing Fig. 2(a), where the simulations included PVG, to Fig. 2(b), where it is neglected.

Impact of electromagnetic effects.—Here we present the significant impact of electromagnetic stabilization. Linear and nonlinear β_e scans based on discharge 66404 parameters are shown in Fig. 3. The range of experimental β_e values (0%–0.5%) lies significantly below the computed kinetic ballooning mode thresholds. Electromagnetic effects lead to linear ITG mode stabilization with increasing β_e [22]. For our parameters, this leads to a growth rate reduction of $\approx 25\%$ at $\beta_e = 0.5\%$, at the upper range of our experimental β_e values. The degree of linear ITG mode stabilization, i.e., the relative reduction of γ for $\beta_e > 0$ compared with $\beta_e = 0$, is stronger as R/L_{Ti} is increased. This is consistent with the corresponding increase of the coupling between the electromagnetic shear Alfvén wave and the ITG mode with pressure gradients at any given β_e value [22].

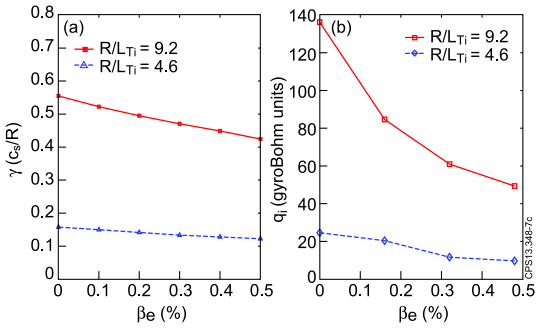

FIG. 3 (color online). Linear growth rates (a) and nonlinear ion heat fluxes (b) calculated in β_e and R/L_{Ti} scans based on discharge 66404 parameters. In the linear scan, $k_y = 0.4$ in units of $1/\rho_s$. Runs included collisions, experimental geometry, two species, and assumed $T_e/T_i = 1$.

A striking observation is that the *nonlinear* electromagnetic ITG stabilization significantly exceeds the linear stabilization, increasing to $\approx 65\%$ as compared with the linear $\approx 25\%$ at the upper range of the experimental β_e values. This is consistent with GENE results reported in Refs. [23–25], which correlated the enhanced nonlinear stabilization with increased relative zonal flow activity and zonal flow effective growth rates. This increase may be related to the predicted increased coupling to zonal flows in the electromagnetic regime [26]. Future work will investigate these dynamics further. We note that the field structures maintain ballooning parity at the higher β_e values and remain consistent with ITG dominated turbulence.

A key point is that the nonlinear electromagnetic stabilization can be significantly augmented by suprathermal pressure gradients. A parameter of merit for the strength of the electromagnetic impact on the linear ITG mode—to which the nonlinear effect is likely linked—is $\alpha \equiv q^2 \sum_j \beta_j (R/L_{nj} + R/L_{Tj})$, where j sums over all particle species. α is a dimensionless measure of the pressure gradient. We stress that while not an exact parametrization in the general case, α nevertheless captures the qualitative

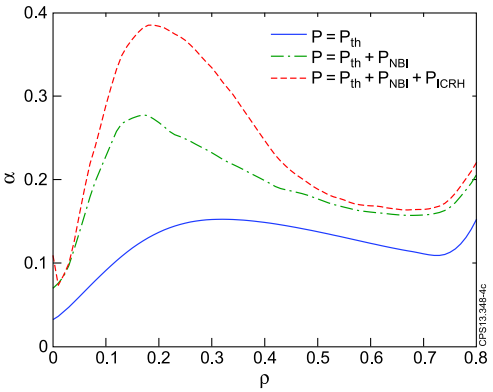

FIG. 4 (color online). The comparative influence of thermal and suprathermal pressure components on α for discharge 66404. Increased α corresponds qualitatively to increased electromagnetic stabilization. The strong influence of suprathermal pressure for $\rho < 0.4$ coincides with the measured low stiffness zone.

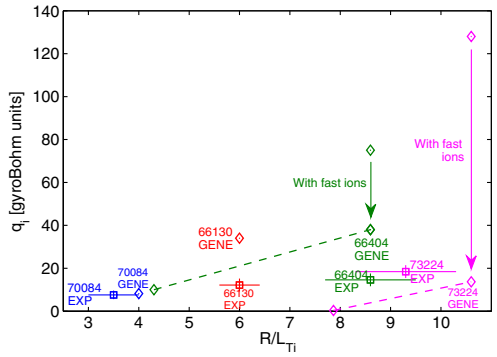

FIG. 5 (color online). Comparison of nonlinear GENE simulations and experimental ion heat flux measurements for the five separate discharges at $\rho = 0.33$. The importance of the fast ion contribution is underlined by the sensitivity studies carried out for discharges 66404 and 73224. The dashed lines connect the results of the nominal 66404 and 73224 simulations with results obtained at reduced R/L_{Ti}.

dependency of the effect on the various relevant parameters [12,22]. For discharge 66 404, the increase in α due to the modeled ICRH and NBI fast ion contributions is shown in Fig. 4. Importantly, the fast ions increase α while simultaneously not contributing to the ITG mode drive. The most significant fast ion contribution to α is at $\rho < 0.4$, coinciding with the decreased stiffness zone in the experiments [13].

The importance of the suprathermal pressure in reproducing the experimental results is seen in Fig. 5. These simulations constitute the full comparison with the experiments and minimize the simplifying assumptions. Electromagnetic effects, collisions, flow shear, realistic T_e/T_i, impurities, fast ions, and experimental geometry are included. The fast ion populations induced by NBI and ICRH are treated as separate hot Maxwellian species, taking the average energy of the slowing-down distributions as the temperatures. For the range of discharges studied, $T_{\text{fast}} = 26$–34 keV for NBI accelerated D, and $T_{\text{fast}} = 20$–23 keV for ICRH accelerated ^{3}He.

For discharge 70084, agreement between the simulation and measurement was reached for input parameters (e.g., R/L_{Ti}) within the confidence intervals of the nominal values. For 73224, agreement was obtained for an input value of R/L_{Ti} 0.3 units beyond the confidence interval. For discharges 66130 and 66404, agreement within a factor of 3 was obtained for simulations with nominal parameters. When removing the fast ions, the ion heat flux for discharge 66404 was increased by a factor of ≈ 2, consistent with Ref. [27]. For 73224 the ion heat flux increased by an order of magnitude. The fast ion stabilization shown here is primarily an electromagnetic stabilization effect, providing significant flux reduction beyond ion dilution and the Shafranov shift stabilization.

The experimentally observed low stiffness is also captured. This is indicated by reduced R/L_{Ti} runs carried out

TABLE II. GENE simulations based on discharge 66404 with collisions, circular geometry, two species, and assumed $T_e/T_i = 1$. The uncertainty values reflect the ion heat flux fluctuations during the saturated state. The electromagnetic stabilization is stronger at low $\hat{s}$, as reflected by the "stabilization factor," which is the ratio between the electromagnetic and electrostatic ion heat fluxes.

β_e [%]	$\hat{s}$	q_i [gyroBohm units]	Stabilization factor
0	0.2	180 ± 14	3.5
0.32	0.2	52 ± 11	
0	0.45	230 ± 14	2.6
0.32	0.45	88 ± 16	
0	0.7	246 ± 26	2.7
0.32	0.7	90 ± 30	

for discharges 66404 and 73224, displayed in Fig. 5. The low stiffness for 73224 is accompanied by an enhanced threshold up-shift, indicated by marginal stability at $R/L_{Ti} = 7.9$, significantly above the linear threshold of $R/L_{Ti,\text{crit}} \approx 2.5$. This is consistent with Ref. [24], where a threshold shift was accompanied by a stiffness reduction for $\beta_e > 0$. The seeming lack of threshold modification for discharge 66404 is attributed to residual activity of trapped electron modes, destabilized by the higher R/L_n and observed at low R/L_{Ti} in linear analysis of this discharge.

The remaining discrepancies in the flux values between the various simulations and measurements can be reconciled by reasonable variations of the input parameters—such as R/L_{Ti}, T_e/T_i, $\hat{s}$, q, and Z_{eff}—within the experimental uncertainties. $Z_{\text{eff}} \equiv (\sum Z_j^2 n_j)/n_e$ is the effective ion charge. However, the discrepancies observed when *not* including the fast ions in an electromagnetic framework are clearly outside this envelope.

We note that discharges in the "high stiffness" branch were also investigated. The significantly lower thermal and suprathermal pressure gradients led to a much reduced impact on the ion heat flux and stiffness reduction compared with the low stiffness branch. This is consistent with the electromagnetic stabilization mechanism being primarily responsible for the splitting of the experimental data into two separate stiffness branches.

Finally, the impact of the electromagnetic stabilization is stronger at low $\hat{s}$. This is shown in Table II. The simulations—based on discharge 66404—used circular geometry with $q = 1.7$. This $\hat{s}$ dependence of the electromagnetic stabilization is in qualitative agreement with the experimentally observed decreased stiffness at low $\hat{s}$.

Summary and implications.—Based on gyrokinetic simulations with the GENE code, nonlinear electromagnetic stabilization of ITG modes by both thermal and suprathermal pressure gradients is shown to be the key factor leading to a reduced ion temperature profile stiffness regime at JET. This mechanism provides a clear explanation for the observations. The previously hypothesized

mechanism of concomitant low magnetic shear and high rotational flow shear is shown to be insufficient to lead to significant stiffness reduction. The electromagnetic stabilization is also seen to be more effective at low magnetic shear, in line with the experimental trends.

This effect has striking consequences for burning plasma tokamak scenarios, where for larger devices flow shear is expected to be low, but the fast ion component from fusion-α particles will be significant. Evidence of such improved ion energy confinement in JET DT plasmas has been seen [28,29]. The increased strength of the effect at low $\hat{s}$ indicates a more favorable energy confinement extrapolation for burning hybrid scenarios, which contain a significant volume of low $\hat{s}$. Furthermore, hybrid scenarios contain a higher suprathermal pressure fraction than ''standard'' scenarios, owing to reduced density due to lower current. DT hybrid scenarios at JET may thus achieve improved energy confinement beyond what has been observed in DD discharges. For ITER, this beneficial effect may relax the constraints on pedestal performance and heating and current drive requirements for achieving the scenario, as determined from previous extrapolations [30]. Finally, in the JET stiffness experiments performed until now, flow shear and suprathermal pressure gradients were cocorrelated. This calls for additional experiments, on various machines, to decouple the impact of these parameters on transport.

This work, supported by the European Communities under the contract of Association between EURATOM/FOM, was carried out within the framework of the European Fusion Programme with financial support from NWO. This work is supported by NWO-RFBR Centre-of-Excellence on Fusion Physics and Technology (Grant No. 047.018.002). This work is part of the research program ''Fellowships for Young Energy Scientists'' (YES!) of the Foundation for Fundamental Research on Matter (FOM), which is financially supported by the Netherlands Organisation for Scientific Research (NWO). The authors would like to thank C. Angioni, H. Doerk, R. Dumont, D. R. Hatch, E. Highcock, F. Millitello, F. Ryter, A. Schekochihin, M. Schneider, J. Weiland, and E. Westerhof for stimulating discussions. Resources of HPC-FF in Jülich are gratefully acknowledged. This research used computational resources at the National Research Scientific Computing Center, which is supported by the Office of Science of the U.S. Department of Energy under Contract No. DE-AC02-05CH11231. The authors are grateful to D. R. Mikkelsen for assistance. This work was done under the JET-EFDA work programme [31].

*Corresponding author.
J.Citrin@differ.nl

[1] E. J. Doyle *et al.*, Nucl. Fusion **47**, S18 (2007).
[2] F. Romanelli, Phys. Fluids B **1**, 1018 (1989).
[3] P. Diamond, S.-I. Itoh, K. Itoh, and T. S. Hahm, Plasma Phys. Controlled Fusion **47**, R35 (2005).
[4] E. Joffrin *et al.*, Nucl. Fusion **45**, 626 (2005).
[5] J. Hobirk *et al.*, Plasma Phys. Controlled Fusion **54**, 095001 (2012).
[6] P. Mantica *et al.*, Phys. Rev. Lett. **102**, 175002 (2009).
[7] P. Mantica *et al.*, Phys. Rev. Lett. **107**, 135004 (2011).
[8] F. Jenko, W. Dorland, M. Kotschenreuther, and B. N. Rogers, Phys. Plasmas **7**, 1904 (2000); See http://gene.rzg.mpg.de for code details and access.
[9] G. Tardini *et al.*, Nucl. Fusion **47**, 280 (2007).
[10] C. Holland *et al.*, Phys. Plasmas **18**, 056113 (2011).
[11] C. Bourdelle, G. T. Hoang, X. Litaudon, C. M. Roach, and T. Tala, Nucl. Fusion **45**, 110 (2005).
[12] M. Romanelli, A. Zocco, F. Crisanti, and JET-EFDA Contributors, Plasma Phys. Controlled Fusion **52**, 045007 (2010).
[13] F. Ryter *et al.*, Nucl. Fusion **51**, 113016 (2011).
[14] M. Schneider, L.-G. Eriksson, I. Jenkins, J. F. Artaud, V. Basiuk, F. Imbeaux, T. Oikawa, JET-EFDA Contributors, and ITM-TF Contributors, Nucl. Fusion **51**, 063019 (2011).
[15] J. Hedin, T. Hellsten, L.-G. Eriksson, and T. Johnson, Nucl. Fusion **42**, 527 (2002).
[16] J. F. Artaud *et al.*, Nucl. Fusion **50**, 043001 (2010).
[17] J. Candy, R. E. Waltz, and W. Dorland, Phys. Plasmas **11**, L25 (2004).
[18] B. F. McMillan, X. Lapillonne, S. Brunner, L. Villard, S. Jolliet, A. Bottino, T. Görler, and F. Jenko, Phys. Rev. Lett. **105**, 155001 (2010).
[19] X. Lapillonne, S. Brunner, T. Dannert, S. Jolliet, A. Marinoni, L. Villard, T. Görler, F. Jenko, and F. Merz, Phys. Plasmas **16**, 032308 (2009).
[20] J. E. Kinsey, R. E. Waltz, and J. Candy, Phys. Plasmas **12**, 062302 (2005).
[21] E. G. Highcock, A. A. Schekochihin, S. C. Cowley, M. Barnes, F. I. Parra, C. M. Roach, and W. Dorland, Phys. Rev. Lett. **109**, 265001 (2012).
[22] J. Y. Kim, W. Horton, and J. Q. Dong, Phys. Fluids B **5**, 4030 (1993).
[23] M. J. Pueschel, M. Kammerer, and F. Jenko, Phys. Plasmas **15**, 102310 (2008).
[24] M. J. Pueschel and F. Jenko, Phys. Plasmas **17**, 062307 (2010).
[25] M. J. Pueschel, T. Görler, F. Jenko, and D. R. Hatch (to be published).
[26] F. Militello, M. Romanelli, J. W. Connor, and R. J. Hastie, Nucl. Fusion **51**, 033006 (2011).
[27] C. Holland, C. C. Petty, L. Schmitz, K. H. Burrell, G. R. McKee, T. L. Rhodes, and J. Candy, Nucl. Fusion **52**, 114007 (2012).
[28] S. E. Sharapov *et al.*, Fusion Sci. Technol. **53**, 989 (2008).
[29] D. Testa and M. Albergante, Europhys. Lett. **97**, 35 003 (2012).
[30] J. Citrin, J. F. Artaud, J. Garcia, G. M. D. Hogeweij, and F. Imbeaux, Nucl. Fusion **50**, 115007 (2010).
[31] See the Appendix of F. Romanelli *et al.*, *Proceedings of the 24th IAEA Fusion Energy Conference 2012, San Diego, USA* [International Atomic Energy Agency (IAEA), Vienna, 2012]. (All the members of the JET-EFDA collaboration appear in the appendix of this paper.)